




Cite this: *RSC Adv.*, 2019, 9, 12990

Sealing effect of surface porosity of Ti–P composite films on tinplates

Ziyu Wang,^a Delong Kong,^a Minghao Wang,^a Guixiang Wang,^b Ning Li ^{*a} and Deyu Li^{*a}

A novel chrome-free Ti–P composite film was prepared by casting a mixed solution containing titanium and phosphorus species, which is able to seal the pores on the tinplate surface. The obtained film was characterized using scanning electron microscopy (SEM), energy dispersive X-ray spectroscopy (EDS), and X-ray photoelectron spectroscopy (XPS). The surface porosity sealing effect on tinplates was verified by using a glow discharge spectrometer (GDS), porosity tests, and XPS. The results show that the film on the tinplates is composed of TiO_2 , $\text{Ti}_3(\text{PO}_4)_4 \cdot n\text{H}_2\text{O}$, and FePO_4 . Micropores on the tinplates are reduced apparently after film deposition, and the content of iron exposed in the pores is decreased significantly. An obvious concentration peak of phosphorus at a depth of around $0.75 \mu\text{m}$ infers that the film can penetrate into the micro-pores. The film lead to a 42.5% decrease in the surface porosity of the tinplates, exhibiting an outstanding surface porosity sealing effect in comparison with pure Ti or P films. Mechanistic analysis using XPS indicates that $\text{Ti}_3(\text{PO}_4)_4 \cdot n\text{H}_2\text{O}$ and FePO_4 in the film play a role in sealing the surface porosity.

Received 23rd December 2018

Accepted 22nd April 2019

DOI: 10.1039/c8ra10523e

rsc.li/rsc-advances

1. Introduction

Tinplates have been widely used for the packaging of foods and beverages.^{1,2} There exist several layers with different compositions on the base steel of a commercially available tinplate in the ideal case.² The innermost layer is Fe–Sn alloy layer, which comes into being during the reflowing process through the permeation of the molten tin into the iron crystal lattice on the base steel.^{3,4} However, due to limited time, the unalloyed tin will form a metallic tin layer on the alloy layer, and a thin oxide layer of tin is generated on the surface of the metallic tin layer.^{5–8} Tin and its oxides are susceptible to oxidation during storage in humid conditions and curing of lacquers at high temperature, resulting in an unacceptable yellow stain.^{7,9} Moreover, the formation of tin sulfide stains in food cans containing protein easily cause food spoilage.^{9,10} Therefore, traditionally, a chromium oxide film is always introduced on the tin oxide layer to protect tin from oxidation, prevent the formation of sulfide, and also, further improve the corrosion resistance of the tinplate.^{11–14}

Furthermore, the surface condition of tinplate is rather complex in light of the surface roughness and defects. The surface of the tinplate is not smooth due to the large roughness of the base steel.^{5,12} The tin coating exhibits locally significant

differences in thickness depending on surface topography of the base steel.^{2,15} Another crucial point is the possible presence of defects such as porosity in the tin layer or the alloy layer.^{2,6,16} Previous studies^{5,15} by means of secondary ion mass spectroscopy analyses have revealed the exposure of Fe–Sn alloy or the base steel through pores on the tinplate, that will cause severe corrosion during storage in humid conditions or usage in food cans.^{16,17} Therefore, a film that can form in the pores and inhibit the corrosion of metals, namely, with a sealing effect on the pores is necessary for the tinplate.

Although the chromium oxide film has demonstrated an excellent controlling effect on the porosity and has been used on the tinplate for a long time,^{17–20} substitutive technologies such as chrome-free conversion film have been developed due to the toxicity of hexavalent chromium in the passivation solution.^{17,21–23} Among researches on chrome-free conversion films, inorganic conversion films and inorganic/organic hybrid films are usually introduced on the tinplate because simplex organic films cannot exhibit a good corrosion performance and are not resistant to high temperature during curing of lacquers, and also, a composite film or multilayer films with complementary performances have become research trends.^{24–29} Considering the pores on the tinplate, strong corrosion resistance of titanium compound film,^{30–32} and beneficial effect of phosphoric acid for iron,^{33,34} a Ti–P (titanium–phosphorus) composite film can be chosen to form a composite conversion film on the tinplate.

In our previous study, a Ti–P composite film was prepared and improved corrosion resistance was noted as a result,³⁵

^aSchool of Chemistry and Chemical Engineering, Harbin Institute of Technology, Harbin 150001, China. E-mail: lideyuhit@163.com; lininghit@263.net

^bCollege of Materials Science and Chemical Engineering, Harbin Engineering University, Harbin 150001, China



however, the mechanism for the improved anti-corrosion performance still remains unclear. Therefore, in this study, the characterization of the film by morphology observation, elemental analysis, and composite analysis will be carried out, and the sealing effect of the film on the micro-pore will be demonstrated.

2. Experimental

Tinplate was fabricated by electroplating on low carbon steel followed by a reflowing process to form the Sn–Fe alloy inter-layer. Electroplating was performed at 1.4 A dm^{-2} for 32 s in a commercial available RONASTAN™ TP-G7 electroplating solution (The Dow Chemical Company, America). The reflowing process was then carried out utilizing the high-frequency induction equipment at a power of 650 W for 0.6 s to around $300 \text{ }^\circ\text{C}$ to form Fe–Sn alloy followed by quenching in $50 \text{ }^\circ\text{C}$ deionized water. The Ti–P composite conversion film was prepared *via* roll coating the aqueous solution (1.5 g L^{-1} TiOSO_4 , 10 mL L^{-1} H_3PO_4 , 15 g L^{-1} H_2O_2 and 0.35 g L^{-1} surfactant) on the tinplate with a wet film thickness of $6 \text{ }\mu\text{m}$ followed by drying in a vacuum oven at $50 \text{ }^\circ\text{C}$ for 90 s.³⁵

Surface morphology characterization and elemental quantification for the tinplate and the conversion film were performed by employing a Helios NanoLab 600i (Thermo Fisher Scientific Inc., America) scanning electron microscope (SEM) coupled with energy dispersive X-ray spectroscopy (EDS). The chemical composition of the conversion film was analyzed by X-ray photoelectron spectroscopy (XPS), using a PHI 5700 ESCA system (Physical Electronics Inc., America) with a monochromatic $\text{Al K}\alpha$ (1486.60 eV) radiation source. The carbon C 1s peak at 284.6 eV was adopted as a reference for charge correction, and a standard Shirley background was used for subtraction.^{36,37} Decomposition of the narrow spectrum was undertaken using CasaXPS software (version 2.3.16) with Marquardt–Levenberg fitting procedure and Gaussian (70%)–Lorentzian (30%) line shape as defined GL (30) in CasaXPS. Depth profile of the elemental content was analyzed with a GDS750A spectrometer (Leco Corporation, America).

Surface porosity sealing effect of the conversion film was verified by determining the amount of iron dissolved from the micro-pores on the tinplate. The tinplate was fixed to the bottom of a cylindrical container with a 2 cm inner diameter opening in the middle of the bottom to expose an area of 3.14 cm^2 . The mixed solution of $30 \text{ mL } 0.66 \text{ mol L}^{-1}$ KSCN, $30 \text{ mL } 0.435 \text{ mol L}^{-1}$ CH_3COOH , $15 \text{ mL } 1 \text{ wt}\%$ H_2O_2 and 23.5 mL deionized water were then added to the container followed by standing at room temperature for 15 min. After that, $1.5 \text{ mL } 50 \text{ vol}\%$ H_2SO_4 solution was further added followed by transferring the solution to another container. Then, the transmittance “T” of the solution was measured at 485 nm using a 721 visible spectrophotometer (Shanghai Precision Science Instrument Co., Ltd., China). The amount of the dissolved iron was calculated by calibration curve $y = 99.78 \exp(-0.195x)$ ($R^2 = 0.9980$), where y represents the transmittance and x represents the amount value of dissolved iron and expressed in milligrams of dissolved iron per dm^2 .

3. Results and discussion

3.1 Surface analysis of the tinplate

Fig. 1 shows the surface morphology of the base steel and the tinplate. It can be seen from Fig. 1a that there exist striations and pits on the surface of the base steel which should be the roll marks formed during the rolling process of the steel.⁵ Fig. 1b shows that striations and pits can still be seen on the surface of the tinplate after electroplating. Meanwhile, it is notable that micro-pores appear on the surface. Since no pores are found on the surface of the base steel (Fig. 1a), the pores are believed to be present in the tin layer. Such pores may result from incomplete coverage of the tin coating.² After reflowing, the micro-pores did not disappear; instead, several micro-pores with larger size appear as shown in Fig. 1c. It indicates that micro-pores can come into being during electroplating or reflowing process. Further study was carried out by elemental analysis to identify the difference in element content in the micro-pores and the normal area.

Fig. 2 shows energy dispersive spectra at a certain area or a point on the tinplate, and the corresponding results of elemental analysis were listed in Table 1. As described above, there are three layers (Fe–Sn alloy, metallic tin, and tin oxides) on the base steel of a tinplate after reflowing. Consequently, tin, iron, and oxygen are detected on tinplate surface by EDS. The testing area and corresponding spectrum are shown in Fig. 2a, and analyses results are shown in and Table 1. It can be seen that the atomic percentage of tin is maximum, and the content ratio of tin to iron (Sn/Fe) is 1.38. At a certain point in the area without pores (Fig. 2b), the ratio becomes to 3.67, which is significantly higher than the overall value of 1.38. It may be due to the existence of the micro-pores where the content of Sn become very low as can be seen from Fig. 2c and d and Table 1. In a certain micro-pore (Fig. 2c), the dominant element becomes Fe and the Sn/Fe content ratio decreases by 94.8% in comparison with the normal area (Fig. 2b), while in another micro-pore (Fig. 2d) the ratio decreases by 97.8%.

The above results demonstrate that micro-pores are present on the surface of tinplate. The content of iron is much higher in micro-pores than in the normal area, indicating that layers of tin and its oxides in the pores are much thinner than that in the normal area. Also, Fe–Sn alloys or the base steels may expose in the pores considering the different layers on the tinplate surface. Due to the evolution of hydrogen occurs during electroplating, micro-pores are inevitable in the tin layer. Meanwhile, the non-uniform distribution of the current density in micro level due to the rough surface of the base steel as shown in Fig. 1a leads to the uneven thickness distribution of the tin coating. During reflowing process, there is less or even no molten tin in the regions with thinner or without tin coating, and the molten tin will be adequately alloyed with iron, resulting in a much thinner tin layer, or the exposure of Fe–Sn alloy or the base steel. Therefore, a protective film with a sealing effect on surface micro-pores is needed on the tinplate.

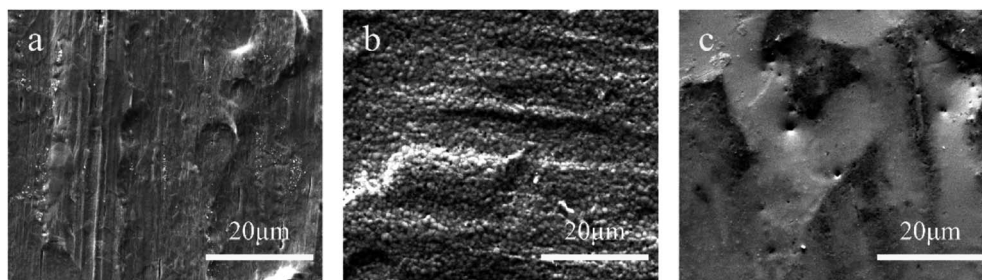


Fig. 1 Surface morphologies of (a) the low carbon steel, (b) tinplate treated with electroplating, and (c) tinplate treated with electroplating and reflowing.

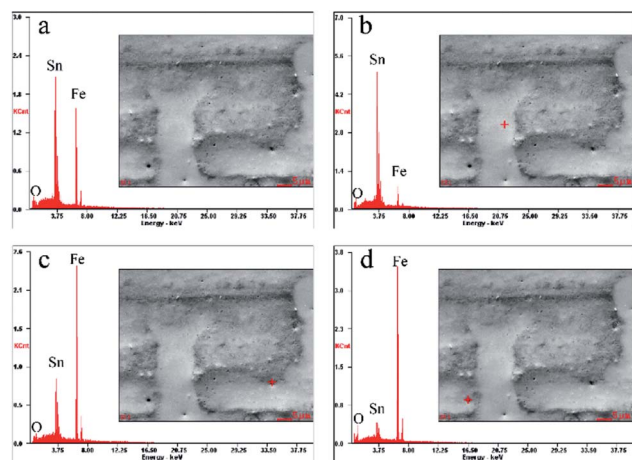


Fig. 2 Energy dispersive spectra from (a) the whole area in the SEM image, (b) a certain point in the normal area, (c) and (d) points in micro-pores.

Table 1 Atomic percentage content (at.%) of surface elements in a certain area or at a certain point corresponding to Fig. 2

Fig. 2	Sn L	Fe K	O K	Sn/Fe
a	54.29	39.31	6.40	1.38
b	69.98	19.08	10.94	3.67
c	15.28	81.48	3.24	0.19
d	6.78	89.84	3.37	0.08

3.2 Characterization of Ti-P composite film on the tinplate

3.2.1 Morphology. Morphology observation for the Ti-P composite film by SEM was firstly performed. For comparative study, a simplex Ti and P compound film were prepared on tinplates with simplex Ti (removing H_3PO_4 in the mixed solution) and P (removing TiOSO_4 and H_2O_2 in the mixed solution) system solution. Surface morphologies of tinplates coated with different conversion films are shown in Fig. 3.

It can be seen from Fig. 3a that several tiny particles are sparsely dispersed on the surface of the tinplate coated with a Ti compound film, whilst micro-pores are still visible. Fig. 3b shows that particles of different sizes and shapes are present on the surface of the tinplate coated with a P compound film.

Among the particles, some larger ones are in the shape of a flat ellipse with a major axis of around $15 \mu\text{m}$. Comparing with Fig. 3a, the particles in Fig. 3b are much larger and distribute more closely. Moreover, no obvious micro-pore can be found. Fig. 3c shows likewise that a large number of particles are present on the surface of the tinplate coated with a Ti-P composite film, and almost no micro-pore. Nevertheless, comparing with Fig. 3b, differences lie in the morphology and size of the particles, which are irregular sphere particles with a smaller size of around $6 \mu\text{m}$. This indicates that the morphology of Ti-P composite film is entirely different from either the simplex Ti or the P compound film. The particles in the composite film are much larger in comparison with the simplex Ti compound film. In contrast, they are finer and more uniform when compared with the individual phosphate films. Also, it can be inferred that the particles could seal the micro-pores on the tinplate surface. Therefore, the particles were further studied through elemental analysis.

3.2.2 Elemental analysis. Elemental analysis of the particles by EDS was performed to identify the content of titanium and phosphorus. The testing area and corresponding spectrum are shown in Fig. 4a and b, respectively. The spectrum from the central region a particle shows that both Ti and P elements are detected. The quantitative calculation result of the spectrum indicates that the atomic percentage of Ti and P elements are 0.26% and 7.73%, respectively. The reason for the low content of Ti is that the concentration of TiOSO_4 in the treatment solution is very low, less than 0.02 mol L^{-1} . The result also shows the presence of the elements O, Sn, and Fe in the central region of the particle. Among all these detected elements, oxygen has the highest atomic percentage content of 73.59%. Since the detection depth of EDS can reach the micron scale, the signal of oxygen may come from the particle or the tin oxide layer. Besides, the content of iron decreases significantly to 7.67%.

From the above results, titanium and phosphorus are detected in the particle, indicating that the particle is composed of compounds of Ti and P. In the presence of particles, the iron content is significantly reduced, indicating a sealing effect of the particles on the surface pores.

3.2.3 Composition analysis. It has been confirmed that both titanium and phosphorus are present at the tinplate surface coated with a Ti-P composite film. Furthermore,

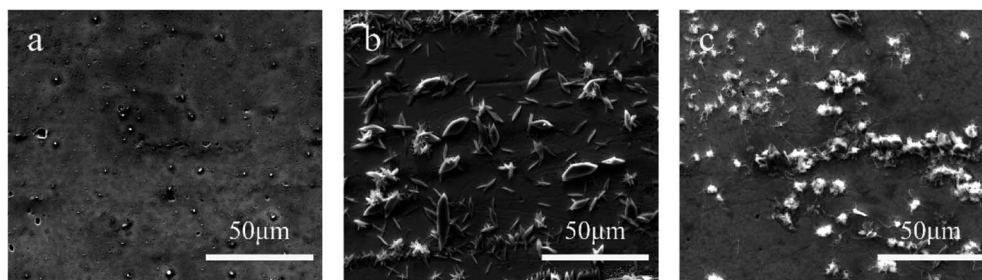


Fig. 3 Surface morphologies of tinplates coated with (a) titanium compound film, (b) phosphate film, and (c) Ti–P composite film.

component analysis for the film was performed by XPS as shown in Fig. 5. For comparative study, analyses for the simplex Ti and P compound films were also performed as shown in Fig. 5a and b, respectively. Fig. 5a shows that the Ti $2p_{3/2}$ peak is located at 458.8 eV, and the separation “ ΔE_b ” between Ti $2p_{3/2}$ and Ti $2p_{1/2}$ peaks is 5.9 eV. Comparing with the standard spectrum of Ti in TiO_2 (Ti $2p_{3/2}$: $E_b = 458.8$ eV, $\Delta E_b = 5.54$ eV),³⁸ it can be inferred that the titanium compound is TiO_2 . In Fig. 5b, the optimized fitting results of P 2p peak shows only one peak at 133.6 eV. When it comes to the standard data of P 2p peak, the ΔE_b between $2p_{3/2}$ and $2p_{1/2}$ is only 0.84 eV,³⁸ that is the overlap of two peaks and are difficult to separate. According to references,^{39,40} it can be deduced that the phosphate film on the tinplate is mainly composed of $FePO_4$. The above results indicate that in the simplex titanium system and phosphorus system, TiO_2 and $FePO_4$ can be formed on the tinplate surface, respectively.

Concerning the film formed in the Ti–P mixed system, the XPS spectra of Ti 2p and P 2p peaks are shown in Fig. 5c and d. In comparison with Fig. 5a, Fig. 5c exhibits a broader Ti $2p_{3/2}$ peak, which can be decomposed into two peaks with $E_b = 458.0$ eV and 459.1 eV, and the ΔE_b between Ti $2p_{3/2}$ and Ti $2p_{1/2}$ is respectively 6.1 eV and 6.2 eV. The differences indicate that the Ti–P composite film contains different compounds of titanium instead of pure TiO_2 . However, the ΔE_b is acceptable which is close to 6.17 eV as reported in reference.³⁸ With regard to the binding energy, Castillo (1996)⁴¹ has reported in his research that the Ti $2p_{3/2}$ peak of TiO_2 is located at 485.0 eV, meanwhile, TiO_2 has been confirmed as a component of the titanium compound film, thus, it can be inferred that TiO_2 is as

well a component of the Ti–P composite film. Hanawa (1991)⁴² has reported in his research that a Ti $2p_{3/2}$ peak located at 459.0 eV is from $Ti_3(PO_4)_4 \cdot nH_2O$, as a reference, the peak with an approximate E_b (459.1 eV) can be seen as from the same substance.

The P 2p peak (see in Fig. 5d) is decomposed into two peaks with $E_b = 133.6$ eV and 134.4 eV, and the ΔE_b between them is 0.8 eV, close to the ΔE_b between P $2p_{3/2}$ and P $2p_{1/2}$ peaks. As described above, the P 2p peak from $FePO_4$ is located at 133.6 eV, and as reported by Hanawa (1991),⁴² the P 2p peak of $Ti_3(PO_4)_4 \cdot nH_2O$ is also with an E_b of 133.6 eV. Combining the analysis for P 2p peak of the phosphate film and Ti 2p peak of the Ti–P composite film, it can be deduced that both $FePO_4$ and $Ti_3(PO_4)_4 \cdot nH_2O$ are the components of Ti–P the composite film. In summary, the film is confirmed to be a composite film of Ti and P compounds, that is TiO_2 , $Ti_3(PO_4)_4 \cdot nH_2O$ and $FePO_4$.

3.3 Sealing effect of the film for the tinplate

3.3.1 GDS depth profile. In the previous studies, a sealing effect of the Ti–P composite film was proposed since micropores on the tinplate were found disappeared after the film formation as shown in Fig. 3d. Given this, investigations will be carried out to verify and further study the sealing effect. The content variation of the elements on the tinplate was firstly examined by GDS. Fig. 6 shows the GDS depth profile of the elements on the tinplate before and after the formation of the Ti–P composite film.

As shown in Fig. 6a, the concentration of iron begins to increase at a depth of 0.5 μm , while the concentration of tin

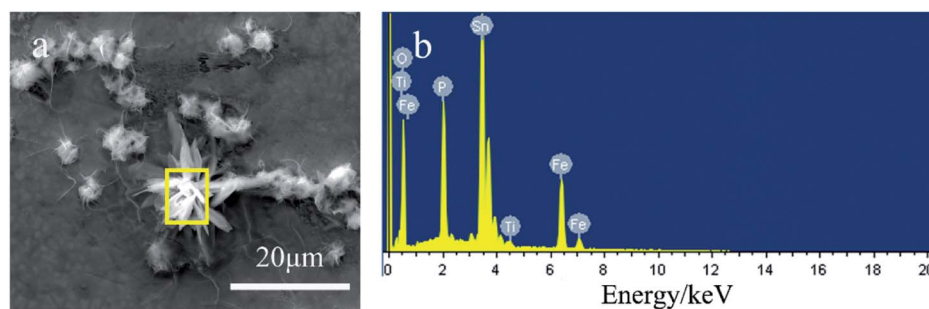


Fig. 4 Elemental analysis of the tinplate coated with a Ti–P composite film, (a) surface morphology of the testing area (b) energy dispersive spectra.

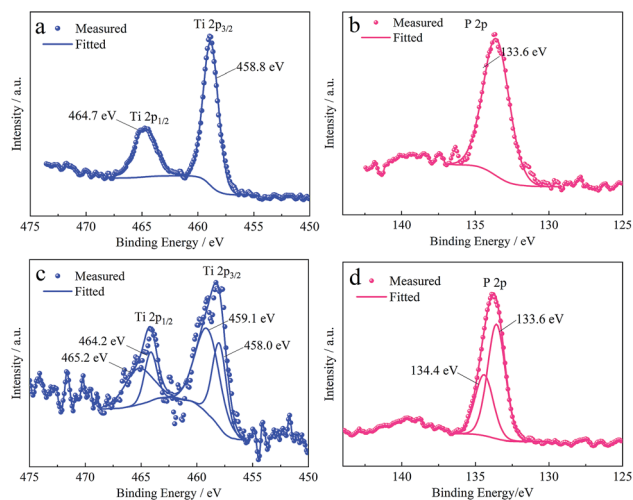


Fig. 5 XPS spectra of Ti 2p and P 2p from the surface of tinplates (a) coated with a titanium compound film, (b) coated with a phosphate film, (c) and (d) coated with a Ti–P composite film.

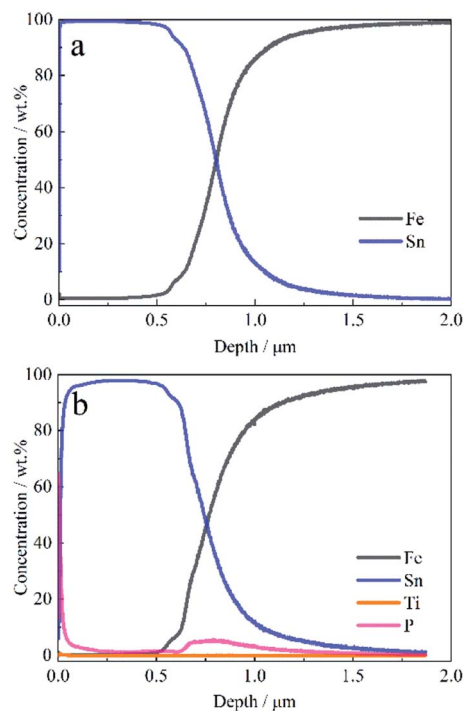


Fig. 6 GDS depth profile of the elements on the tinplate (a) without films, and (b) coated with a Ti–P composition film.

begins to decrease, indicating that the Fe–Sn alloy layer has been reached at this depth. On the surface of the tinplate coated with a Ti–P composite film, the concentration of phosphorus is higher than that of the titanium (see in Fig. 6b), which is corresponding with the results of EDS. Moreover, both the concentrations of Ti and P decrease with depth in the range of 0–0.5 μm . Nevertheless, an obvious concentration peak of phosphorus is present at a depth of around 0.75 μm , and phosphorus is detected to be present in the depth range of 0.6–

1.0 μm . Compared with Fig. 6a, it can be known that the phosphorus in the internal tinplate is derived from the film rather than the base steel. It indicates that the film is also present in the internal tinplate, that is, the film is present in micro-pores and has a sealing effect on the pores.

3.3.2 Porosity test. Porosity test was then carried out to characterize the sealing performance. When the tinplate is placed in a corrosive solution, corrosion of iron and dissolution of iron ions will occur preferentially in micro-pores where the content of iron is at a high level. If a weakly corrosive solution is used and the corrosion time is limited, corrosion of the other regions can be avoided, and iron dissolution from micropores can be selectively achieved. Given this, acetic acid is chosen as the corrosive component, hydrogen peroxide as the oxidant for Fe^{2+} , and KSCN as the color-developing agent in the corrosive solution. After corrosion for 15 min, a small amount of sulfuric acid is added to the solution to prevent colloid formation. Then, the amount of the dissolved iron can be determined *via* spectrophotometry – the less the amount of dissolved iron, the lower the porosity and the better the sealing effect.

Table 2 exhibits the results of porosity tests for the tinplates. Three different regions are selected randomly for parallel testing, and the average was calculated. As exhibited in Table 2, there are no distinct changes on the porosity of the tinplate coated with a titanium compound film (mainly TiO_2 , see the previous study) in comparison with that of the tinplate without a conversion film. According to previous studies, the content of Ti on the tinplate is low, and tiny particles sparsely dispersed at the surface. Therefore, the sealing effect of the film is limited, resulting in a slight decrease of 2.3% in the average. The average of the tinplate coated with a phosphate film decreases by 12.7% compared with that of the tinplate without a conversion film, indicating a better sealing effect than the titanium compound film. It is because the iron on the tinplate has reacted with phosphoric acid to form a film of which the main component is FePO_4 , and several larger particles distributed on the surface as shown in Fig. 3c where no obvious micro-pores can be found. When it comes to the tinplate coated with a Ti–P composite film, the average decreases by 42.5%, implying that the composite film has a significant improvement in sealing effect. It is known from the morphology and composition of the film mentioned above that the composite film is quite different from the simple Ti and P compound films. The particles in the composite film are finer and more uniform in size, and the reaction of Ti and P components generates a new composition of $\text{Ti}_3(\text{PO}_4)_4 \cdot n\text{H}_2\text{O}$, which significantly improves the sealing effect of the composite film. Therefore, the Ti–P composite film has an outstanding surface porosity sealing effect.

3.3.3 Mechanism analysis. As described in the preceding study, ultrathin layers of tin and its oxides, as well as Fe–Sn alloy and the base steel, may be present in micro-pores. In the first case mentioned above, there is no difference in the formation of the film in a pore and a normal area on the tinplate surface. However, in the latter two cases, the formation of the film on the alloy layer and the base steel needs to be investigated. The Fe–Sn alloy layer was prepared by immersing the reflowing tinplate in an etching solution (50 g L^{-1} NaOH and 10 g L^{-1} KIO_3)⁶ for

Table 2 Results of porosity test on tinplates without or with different conversion films (mg dm^{-2})

Tinplate sample	Region 1	Region 2	Region 3	Average
Without films	13.71	14.22	14.01	13.980
With a titanium compound film	14.13	13.26	13.58	13.657
With a phosphate film	12.59	12.17	11.85	12.203
With a Ti-P composite film	7.19	8.23	8.69	8.037

30 min at room temperature. Films were prepared on the Fe–Sn alloy and the base steel *via* the same process as the preparation of Ti–P composite film on the tinplate. XPS spectra of Ti 2p and P 2p peaks are shown in Fig. 7.

Fig. 7a shows Ti $2p_{3/2}$ peak can be fitted with only one peak located at 459.0 eV, which means the titanium is present mainly in the form of $\text{Ti}_3(\text{PO}_4)_4 \cdot n\text{H}_2\text{O}$ on the surface of Fe–Sn alloy according to the preceding XPS analysis. As shown in Fig. 7b, the P 2p peak is decomposed into two peaks with E_b of 133.3 eV and 134.1 eV, respectively. Although the binding energy of P 2p shifts 0.3 eV in comparison with that in Fig. 5d, from the ΔE_b (0.8 eV) and the Ti 2p peaks, it can be inferred that phosphorus is present in the form of $\text{Ti}_3(\text{PO}_4)_4 \cdot n\text{H}_2\text{O}$ and FePO_4 on the surface of Fe–Sn alloy. From the Ti 2p peak, as shown in Fig. 7c, it is known that the content of titanium on the surface of the base steel is very low since the signal is weak and interfered. The E_b (458.9 eV) of Ti $2p_{3/2}$ and the ΔE_b (5.7 eV) are close to those in Fig. 7a, indicating that the titanium is as well derived from the $\text{Ti}_3(\text{PO}_4)_4 \cdot n\text{H}_2\text{O}$. Also, Fig. 7d shows a similar decomposition result of P 2p peak to Fig. 7b. Thus, the same conclusion can be drawn as well. In summary, the Ti–P composite film can be formed both on the surface of the Fe–Sn alloy and the base steel, and the composition of both the films are $\text{Ti}_3(\text{PO}_4)_4 \cdot n\text{H}_2\text{O}$ and FePO_4 . The Ti–P mixed system can also form a film in the pores where the alloy layer or the base steel expose. As a result, the surface porosity of the tinplate decreases.

Nevertheless, it is notable that the composition of the films on the Fe–Sn alloy and the base steel is different from that of the film on the normal tinplate as the absence of the component TiO_2 . Combining the results of the morphology and porosity of the tinplate coated with a TiO_2 film as shown in Fig. 3b and Table 2, it can be deduced that the TiO_2 in the Ti–P composite film does not have a sealing effect on the micro-pores.

Changes in the composition of tin and iron compounds involved in the reaction of the film formation were investigated by XPS to study the mechanism of the formation and sealing effect of the film further. Fig. 8a shows the Sn 3d spectra from the surface of the tinplate without a conversion film. The Sn $3d_{5/2}$ peak is decomposed into two peaks which are located at 486.0 eV and 484.1 eV, and the corresponding ΔE_b between $3d_{5/2}$ and $3d_{3/2}$ peaks are 0.84 eV and 0.85 eV, respectively. The former decomposed peak is derived from SnO according to the reference,³⁸ and the latter is considered to be the peak of metallic tin since the outer layers of tinplate are the tin oxide and metallic tin as described above. After the formation of the Ti–P composite film, the peak position of Sn $3d_{5/2}$ peak shifts positively by 0.8 eV as shown in Fig. 8b, and the decomposed peak at the corresponding position of the metallic tin almost disappear. As reported by Choi,⁴³ the Sn $3d_{5/2}$ peak located at 486.75 eV with a ΔE_b of 8.42 eV is derived from SnO_2 . In comparison, the Sn $3d_{5/2}$ peak located at 486.8 eV with a ΔE_b of 8.4 eV as shown

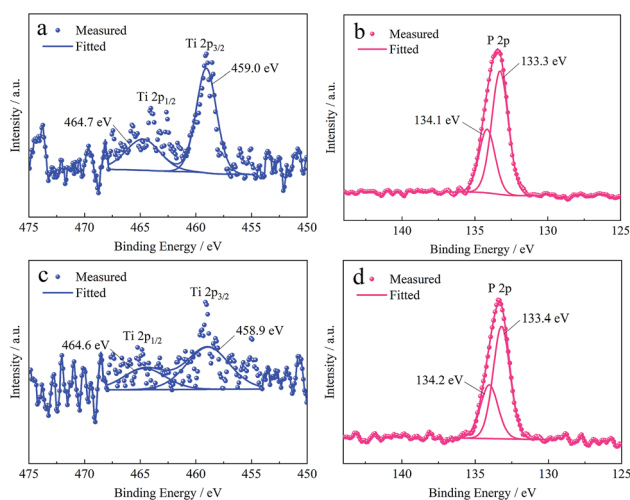


Fig. 7 XPS spectra of Ti 2p and P 2p from the surface of (a), (b) Fe–Sn alloy and (c), (d) base steel treated with Ti–P mixed system, respectively.

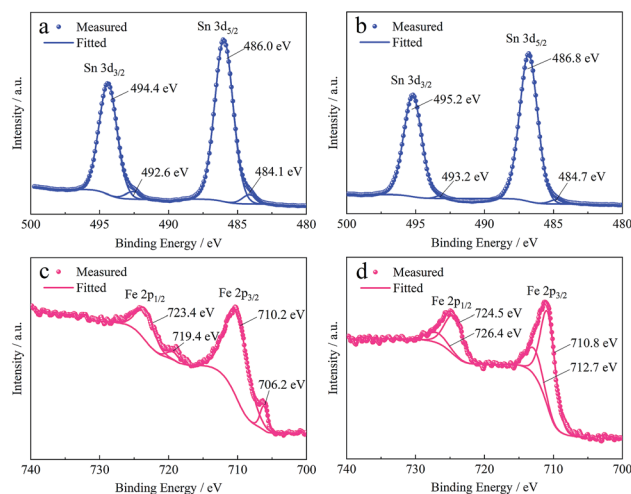


Fig. 8 XPS spectra of Sn 3d from the surface of the tinplate (a) without films and (b) with a Ti–P composite film; XPS spectra of Fe 2p from the surface of the base steel (c) without films and (d) with a Ti–P composite film.

in Fig. 8b is from SnO₂. It indicates that the tin oxide was further oxidated from SnO to SnO₂ during the formation process of the film.

Changes of iron compounds after the coverage of the film were investigated on the base steel since iron was present in the inner layer and cannot be detected using XPS at the surface of the tinplate. Fig. 8c shows the Fe 2p spectra from the base steel. As shown in Fig. 8c, the two decomposed peaks in Fe 2p_{3/2} peak are respectively located at 710.2 eV and 706.2 eV, and the ΔE_b between 2p_{3/2} and 2p_{1/2} peaks are both 13.2 eV. The former decomposed peak is considered to be derived from Fe₃O₄ referring to the previous study,⁴⁴ and the latter is believed to be the peak of metallic iron. After the formation of the Ti–P composite film, the peak position of Fe 2p shift positively as shown in Fig. 8d. The two decomposed peaks in Fe 2p_{3/2} peak are located at 712.8 eV and 710.8 eV, and the ΔE_b between 2p_{3/2} and 2p_{1/2} peaks are both 13.7 eV. The two decomposed peaks are considered to be derived from FePO₄ and Fe₃O₄ according to the previous studies,^{45,46} respectively. The results exhibit more Fe(III) compounds are present on the surface, indicating that iron and its compounds are also oxidated during the formation process of the film.

From the above results, it can be deduced that redox reaction occurs during the process of the Ti–P composite film formation on the tinplate. The H₂O₂ in the Ti–P mixed solution which acts as the complexing agent for TiO₂²⁺ has an oxidation effect for the oxides of iron and tin as well. With the consumption of H₂O₂ in the redox reaction, TiO₂²⁺ loses its ligand, resulting in the generation of TiO₂ and Ti₃(PO₄)₄·nH₂O. In the micro-pores on the tinplate, the exposed iron and its oxides can be converted into Fe²⁺ and Fe³⁺ by H⁺ and then generating FePO₄ with the presence of H₂O₂ and PO₄³⁻ in the solution. Thereby, a Ti–P composite film, which composes of TiO₂, Ti₃(PO₄)₄·nH₂O and FePO₄, is formed on the tinplates. The components of Ti₃(PO₄)₄·nH₂O and FePO₄ in the film generate the sealing effect on surface micro-pores.

4. Conclusions

This work reported a novel chrome-free Ti–P composite conversion film on tinplates. The formation process of the film and the possible sealing effect on surface micro-pores have been comprehensively investigated. Morphology characterization shows that the film consists of irregular sphere particles with a size of around 6 μm. The film is mainly composed of TiO₂, Ti₃(PO₄)₄·nH₂O, and FePO₄. Both the number of micro-pores formerly existing on tinplates surface and the exposed iron in micro-pores were significant decreased. GDS examines present an obvious concentration peak of phosphorus at a depth of around 0.75 μm. Porosity tests indicate a decrease in surface porosity by 42.5% after film deposition. The decreased values for individual TiO₂ and FePO₄ films are only 2.3% and 12.7%, respectively. The results reveal that the film can form into micro-pores and show an outstanding sealing effect on the micro-pores. Ti₃(PO₄)₄·nH₂O and FePO₄ in the film are crucial for the sealing effect on the micro-pores exposed Fe–Sn alloy and/or the base steel. Both oxidations from SnO to SnO₂ and

from iron to Fe(III) occur during the formation of the film. This study has solved the surface porosity problem of tinplates by using the newly invented Ti–P composite film.

Conflicts of interest

There are no conflicts to declare.

References

- 1 S. Blunden and T. Wallace, *Food Chem. Toxicol.*, 2003, **41**, 1651–1662.
- 2 F. C. Caiazza, L. Brambilla, A. Montanari and S. Mischler, *Surf. Interface Anal.*, 2018, **50**, 430–440.
- 3 H. E. Biber, *J. Electrochem. Soc.*, 1966, **113**, 362–365.
- 4 H. E. Biber and W. Harter, *J. Electrochem. Soc.*, 1966, **113**, 828–834.
- 5 S. Ramamurthy, T. L. Walzak, S. F. Lu, T. C. Lipson and N. S. McIntyre, *Surf. Interface Anal.*, 1991, **17**, 834–841.
- 6 G. F. Cui, J. H. Wang, N. Li and X. Q. Huang, *Mater. Chem. Phys.*, 2006, **97**, 488–493.
- 7 T. Y. Kim, Y. S. Jin and K. Y. Kim, *Surf. Coat. Technol.*, 1998, **99**, 319–325.
- 8 A. N. Grassino, Z. Grabaric, A. Pezzani, G. Fasanaro and A. Lo Voi, *Food Chem. Toxicol.*, 2009, **47**, 1556–1561.
- 9 M. C. Biermann, PhD thesis, University of Pretoria, Pretoria, 2005.
- 10 N. Mora, E. Cano, J. L. Polo, J. M. Puente and J. M. Bastidas, *Corros. Sci.*, 2004, **46**, 563–578.
- 11 S. Chen, L. Xie and F. Xue, *Appl. Surf. Sci.*, 2013, **276**, 454–457.
- 12 M. Wang, Z. Wang, D. Li and N. Li, *Coatings*, 2018, **8**, 94.
- 13 S. C. Britton and J. C. Sherlock, *Br. Corros. J.*, 1974, **9**, 96–102.
- 14 P. Rocquet and P. Aubrun, *Br. Corros. J.*, 1970, **5**, 193–197.
- 15 S. F. Lu, G. R. Mount, N. S. McIntyre and A. Fenster, *Surf. Interface Anal.*, 1994, **21**, 177–183.
- 16 J. G. Huang, N. Li and D. R. Zhou, *J. Cent. South Univ. Technol.*, 2004, **11**, 362–366.
- 17 M. A. Arenas, A. Conde and J. J. de Damborenea, *Corros. Sci.*, 2002, **44**, 511–520.
- 18 J. M. Bastidas, J. M. Cabanes and R. Catala, *Prog. Org. Coat.*, 1997, **30**, 9–14.
- 19 E. Zumelzu and C. Cabezas, *Mater. Charact.*, 1995, **34**, 143–148.
- 20 R. Neish and J. Donelson, *Food Technol.*, 1960, **14**, 37–42.
- 21 X. Huang and N. Li, *Appl. Surf. Sci.*, 2007, **254**, 1463–1470.
- 22 D. Alvarez, A. Collazo, X. R. Novoa and C. Perez, *Prog. Org. Coat.*, 2014, **77**, 2066–2075.
- 23 D. Alvarez, A. Collazo and C. Perez, *Surf. Coat. Technol.*, 2017, **321**, 108–117.
- 24 Y. Kiyota and M. Matsunaga, *ECS Trans.*, 2008, **11**, 43–46.
- 25 E. Almeida, N. De Cristofaro, N. Mora, J. M. Bastidas and J. M. Puente, *JCT Res.*, 2004, **1**, 103–109.
- 26 D. Yfantis, A. Yfantis, B. Tzalas and D. Schmeisser, *Corrosion*, 2000, **56**, 700–708.

- 27 S. R. Kunst, L. V. R. Beltrami, H. R. P. Cardoso, J. A. Santana, V. H. V. Sarmento, I. L. Müller and C. D. F. Malfatti, *Mater. Res.*, 2015, **18**, 151–163.
- 28 E. K. K. Baldin, S. R. Kunst, L. V. R. Beltrami, T. M. Lemos, M. C. Quevedo, A. C. Bastos, M. G. S. Ferreira, P. R. R. Santos, V. H. V. Sarmento and C. D. F. Malfatti, *Thin Solid Films*, 2016, **600**, 146–156.
- 29 S. R. Kunst, H. R. P. Cardoso, C. T. Oliveira, J. A. Santana, V. H. V. Sarmento, I. L. Muller and C. F. Malfatti, *Appl. Surf. Sci.*, 2014, **298**, 1–11.
- 30 X. Huang and N. Li, *J. Alloys Compd.*, 2008, **465**, 317–323.
- 31 E. Almeida, M. R. Costa, N. De Cristofaro, N. Mora, R. Catalá, J. M. Puente and J. M. Bastidas, *Corros. Eng., Sci. Technol.*, 2005, **40**, 158–164.
- 32 R. Catala, M. Alonso, R. Gavara, E. Almeida, J. M. Bastidas, J. M. Puente and N. de Cristaforo, *Food Sci. Technol. Int.*, 2005, **11**, 223–227.
- 33 A. Ragheb and L. A. Kamel, *Corrosion*, 1962, **18**, 153t–157t.
- 34 T. Ohga, H. Miyazaki and M. Yamamoto, *Zairyo to Kankyo*, 1997, **46**, 771–776.
- 35 Z. Wang, M. Wang, D. Li and N. Li, *J. Electrochem.*, 2018, **24**, 13–19.
- 36 T. Yamashita and P. Hayes, *Appl. Surf. Sci.*, 2008, **254**, 2441–2449.
- 37 M. C. Biesinger, B. P. Payne, L. W. M. Lau, A. Gerson and R. S. C. Smart, *Surf. Interface Anal.*, 2009, **41**, 324–332.
- 38 J. F. Moulder, *Handbook of X-ray photoelectron spectroscopy*, 1995.
- 39 Y. Barbaux, M. Dekioux, D. Lemaguer, L. Gengembre, D. Huchette and J. Grimblot, *Appl. Catal., A*, 1992, **90**, 51–60.
- 40 R. Franke, T. Chasse, P. Streubel and A. Meisel, *J. Electron Spectrosc. Relat. Phenom.*, 1991, **56**, 381–388.
- 41 R. Castillo, B. Koch, P. Ruiz and B. Delmon, *J. Catal.*, 1996, **161**, 524–529.
- 42 T. Hanawa and M. Ota, *Biomaterials*, 1991, **12**, 767–774.
- 43 W. K. Choi, H. J. Jung and S. K. Koh, *J. Vac. Sci. Technol., A*, 1996, **14**, 359–366.
- 44 B. J. Tan, K. J. Klabunde and P. M. A. Sherwood, *Chem. Mater.*, 1990, **2**, 186–191.
- 45 D. D. Hawn and B. M. Dekoven, *Surf. Interface Anal.*, 1987, **10**, 63–74.
- 46 P. Mills and J. L. Sullivan, *J. Phys. D: Appl. Phys.*, 1983, **6**, 723.